High-performance giant magnetoresistive sensorics on flexible Si membranes

Nicolás Pérez, Michael Melzer, Denys Makarov, et al.

View Online   **Export Citation**   **CrossMark**

ARTICLES YOU MAY BE INTERESTED IN

High-performance giant magnetoresistive sensorics on flexible Si membranes

Nicolás Pérez,[1,a)] Michael Melzer,[1] Denys Makarov,[1] Olaf Ueberschär,[2] Ramona Ecke,[2] Stefan E. Schulz,[2,4] and Oliver G. Schmidt[1,3]

[1]*Institute for Integrative Nanosciences, IFW Dresden, Helmholtzstrasse 20, 01069 Dresden, Germany*
[2]*Fraunhofer Institute for Electronic Nano Systems ENAS, Technologie-Campus 3, 09126 Chemnitz, Germany*
[3]*Material Systems for Nanoelectronics, TU Chemnitz, Reichenhainer Straße 70, 09107 Chemnitz, Germany*
[4]*Center for Microtechnologies, TU Chemnitz, Reichenhainer Straße 70, 09107 Chemnitz, Germany*

We fabricate high-performance giant magnetoresistive (GMR) sensorics on Si wafers, which are subsequently thinned down to 100 μm or 50 μm to realize mechanically flexible sensing elements. The performance of the GMR sensors upon bending is determined by the thickness of the Si membrane. Thus, bending radii down to 15.5 mm and 6.8 mm are achieved for the devices on 100 μm and 50 μm Si supports, respectively. The GMR magnitude remains unchanged at the level of $(15.3 \pm 0.4)\%$ independent of the support thickness and bending radius. However, a progressive broadening of the GMR curve is observed associated with the magnetostriction of the containing $Ni_{81}Fe_{19}$ alloy, which is induced by the tensile bending strain generated on the surface of the Si membrane. An effective magnetostriction value of $\lambda_s = 1.7 \times 10^{-6}$ is estimated for the GMR stack. Cyclic bending experiments showed excellent reproducibility of the GMR curves during 100 bending cycles. © 2015 Author(s). All article content, except where otherwise noted, is licensed under a Creative Commons Attribution 3.0 Unported License. [http://dx.doi.org/10.1063/1.4918652]

Flexible electronics[1–4] is a rapidly evolving field that has given rise to new integration possibilities of electronic circuitry for applications requiring mechanical stress and deformation, such as flexible displays,[5] electronic skin,[6,7] biomedical applications,[8,9] and energy harvesting devices.[10] The family of flexible devices will not be complete without navigation modules, body tracking, and position monitoring systems. All these tasks are typically solved by means of magnetic field sensorics. In this respect, the smart combination of metallic thin films deposited directly on polymeric supports allowed to fabricate flexible Hall sensors[11] as well as flexible and even stretchable magnetoelectronics relying on the giant magnetoresistance (GMR) effect in multilayers[12–14] and spin valves[15,16] or on the tunnel magnetoresistance in magnetic tunnel junctions.[17,18] These flexible devices are already successfully integrated in fluidic systems,[19] applied as pointing devices and proximity sensorics[11,20] and act as components of printed electronics.[21,22] Integrated into smart skins, these magneto-sensory systems equip the recipient with a so called *sixth sense* able to perceive the presence of static or dynamic magnetic fields for orientation and manipulation aids.[20]

The integration of flexible sensing elements with on-site signal conditioning electronics is challenging on polymeric substrates. This, however, is crucial for high precision sensorics in environments with electromagnetic disturbances. This issue could be overcome by combining high-performance metal-based GMR sensorics with thin Si membranes accommodating integrated CMOS circuitry. The key question, which has to be addressed when fabricating such a hybrid device, is its performance under mechanical deformation. In

this respect, the functioning of integrated circuitry on non-thinned (675 μm) Si wafers upon bending down to 400 mm radius (corresponding to a stress of 150 MPa) has been studied, revealing only few percent variations in the transistor parameters.[23] Wafer scale CMOS circuitry on ultra-thin 6 nm Si membranes obtained by controlled spalling technology has been shown to be fully functional at bending radii of 6.3 mm.[24] Bending tests of GMR sensorics prepared on 330–380 μm thick SiO_x wafers[25,26] or 250 μm glass slides[27] were carried out to study effects of inverse magnetostriction on the magnetoelectric characteristics[27] and eventually to use those for highly sensitive strain gauges.[25,26] The used thick supports allow bending radii above 100 mm only. Due to these large bending radii, it is not possible to assess the applicability of these GMR sensorics for flexible electronics on Si membranes.

Here, we address the impact of the mechanical deformations on the magnetoelectrical performance of the $Ni_{81}Fe_{19}$(Py)/Cu GMR multilayers prepared on 4 in. Si wafers, which are subsequently thinned down to 100 or 50 μm. We report on the minimum bending radii for the samples and their robustness against uninterrupted mechanical deformation tested by reversibly bending the devices. The relevant GMR characteristics, namely, the GMR amplitude, the full width at half maximum (FWHM) of the GMR curve, and the associated slope of its linear part, are monitored. The observed changes in the GMR characteristics are related to strain-induced effects in the magnetic layer stack.

A photolithographic lift-off procedure was applied to pattern GMR multilayer films. The GMR multilayer stacks of Py(1.6 nm)/30×[Py(1.6 nm)/Cu(2.3 nm)] with a total thickness of 108.6 nm were deposited using DC magnetron sputtering on the naturally oxidized [100] surface of 4 in. Si wafers. Sputtering of the $Ni_{80}Fe_{20}$ target material results in a

a)n.perez.rodriguez@ifw-dresden.de

composition shift in the resultant alloy film to $Ni_{81}Fe_{19}$. In the following, we shall use Py as a convenient abbreviation for $Ni_{81}Fe_{19}$, keeping in mind a non-zero magnetostriction of this alloy.[28] In particular, for $Ni_{81}Fe_{19}$ *thin films*, increased values of the saturation magnetostriction, λ_s, are attributed to interfacial effects.[29] The front side of the 4 in. wafers was attached to a UV tape. Held in an 8 in. frame, these wafers were thinned from their backside to a remaining thickness of $100\,\mu m$ using a coarse grinding wheel. Subsequently, some of the wafers were further thinned by means of a fine wheel to a thickness of $50\,\mu m$. All grinding processes were performed on a DISCO DAG 810 device. After thinning, the wafers were transferred from the UV tape onto a dicing tape, thereby enabling the dicing along [100] crystallographic planes into separate rectangular sensor test structures (Figs. 1(a)–1(c)). The lateral dimensions of the diced Si supports were 5 mm × 18 mm and the 1 mm × 16 mm sensor stripes had four contact pads to allow reliable resistance measurements under applied field (Fig. 1(e), inset). The GMR sensors were contacted in a four-point configuration using silver paste and Cu wire of $200\,\mu m$ in diameter (Fig. 1(e), inset). The GMR curves of the samples on $100\,\mu m$ and $50\,\mu m$ thick Si membranes are rather similar to the reference samples on $525\,\mu m$ non-thinned wafers (Fig. 1(e)). The GMR ratio is defined as $\Delta R/R = (R - R_{sat})/R_{sat}$, where R is the electrical resistance of the sample in an applied magnetic field and R_{sat} is

the value of the electrical resistance when the GMR stack is magnetically saturated. Bending experiments were carried out using a computer-controlled motorized stage, which was placed in between the poles of an electromagnet (Fig. 2(a)). The samples were positioned in such a way that the multi-layer structure was bent along its long axis and in a direction perpendicular to the applied magnetic field. For the bending tests, the samples were clamped on the stage using additional Scotch Tape underneath as shown in Fig. 2(b). Both ends of the tape were held into the clamps; hence, stress could be applied to the samples laterally (Fig. 1(d)). The distance between the clamps was successively reduced in steps of $50\,\mu m$ causing the samples to bend (Fig. 2(c)). The resistance was measured at the central region, where the curvature is most pronounced. The bending radii, r, were evaluated in the segment between the two central contacts using calibrated photographs and image processing software. The obtained values for r are given within 3% uncertainty. As sketched in Fig. 1(d), the bending of the sample generates a tensile stress on the upper part of the Si membrane and subsequently on the GMR multilayer stack.
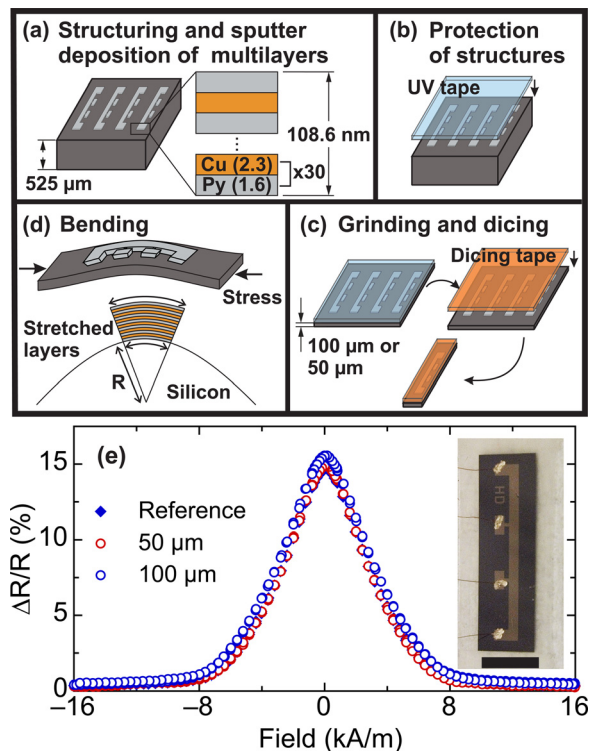

FIG. 1. Schematics showing the fabrication steps of the GMR sensorics on Si membranes: (a) deposition and structuring of the GMR stack on rigid Si wafers. (b) The samples are protected using UV tape. (c) The Si wafer is ground down to the thickness of 50 or $100\,\mu m$ followed by dicing the samples into separate structures of 5 mm × 18 mm. (d) Scheme depicting deformation of the Si membranes and stretching of the layers under applied stress. (e) GMR curves of a reference sample on the rigid Si wafer and of the samples on 50 and $100\,\mu m$ thick Si membranes. The samples are measured in the unbent state. Inset in (e) shows a photograph of the sensor, the black bar corresponding to 5 mm.
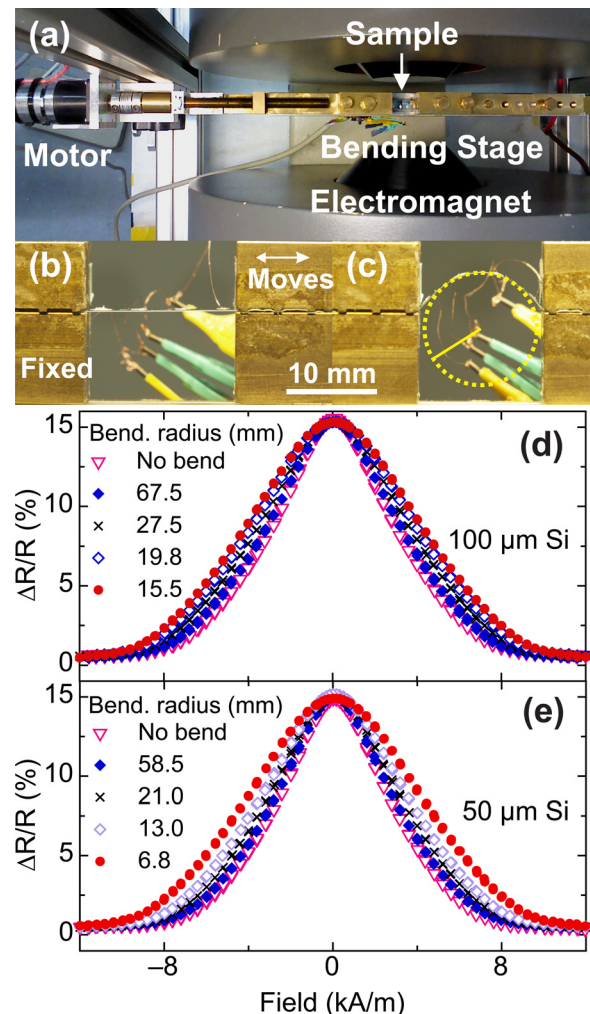

FIG. 2. Performance of the sample upon mechanical deformation: (a) Sample mounted on a motorized bending stage located between the pole shoes of the electromagnet. Close-up of the sample area showing (b) unbent sample and (c) sample bent to the radius of 6.8 mm. Contacting clips, Cu wire, and silver paste pads can be seen. GMR curves taken at several bending radii for the samples on Si membranes with a thickness of (d) $100\,\mu m$ and (e) $50\,\mu m$.

GMR measurements were carried out after each bending step, progressively reducing the bending radius until the fracture of the sample (Figs. 2(d) and 2(e)). The minimum radius before fracture observed for the 50 μm thick samples was 6.8 mm; for the 100 μm thick samples, the fracture point was reached at a minimum radius of 15.5 mm. These bending radii are typical for the functional elements prepared on 100–μm-thick flexible foils.[30] Smaller bending radii can be achieved by using thinner flexible foils.[6,20,31] As indicated in Fig. 1(d), the local deformation in the bent Si membrane is considered to increase linearly with the distance from the central neutral mechanical plane, which itself remains unstrained (tensile strain towards the outside and compressive towards the inside).[32,33] Hence, the distinct fracture radii for the samples prepared on 50 and 100 μm thick Si membranes are attributed to the different strain levels at the surfaces of the substrates at a given bending radius-(only half the value for the thinner samples. As the thickness of the support increases, the fracture strain at the outer surface is reached already at a larger bending radius.

Analysis of the data in Figs. 2(d) and 2(e) reveals that the net resistance of the multilayer structures, evaluated at magnetic saturation (40 kA/m) and remanence (zero applied field) increases linearly with curvature, but remains within less than 1% of the initial value (Fig. 3(a)). Remarkably, the GMR ratio remains unchanged at $(15.3 \pm 0.4)\%$ for all the studied bending radii, independent of the thickness of the support. This strain invariance of the GMR magnitude is crucial when designing flexible GMR on-off sensors, e.g., magnetic switches, for flexible electronics.

However, a noticeable broadening of the GMR curves was observed with bending (Figs. 2(d) and 2(e)). Furthermore,

the FWHM increases linearly with curvature, $1/r$, as shown in Fig. 3(b). In addition, we note that the FWHM values extracted from the GMR curves measured for the samples in planar configuration (FWHM $\approx$ 6 kA/m) or just before the breaking point (FWHM $\approx$ 9 kA/m) are rather similar for both support thicknesses (Fig. 3(b)). Keeping in mind that the stress at the free surface of thin Si membranes is proportional to $1/r$,[34] these findings indicate that the FWHM scales solely with the stress experienced by the sample coming from the deformation of the Si support.

Assuming coherent rotation of the magnetization in the Py layers in the GMR stack,[35] the FWHM can be estimated as twice the anisotropy field, H_a. Thus, our experiments reveal a linear increase of the anisotropy field of the GMR multilayer stack with the stress induced on the top surface of the Si support due to bending. This is in line with earlier studies, where the anisotropy field of individual polycrystalline Py thin films was found to be proportional to the curvature.[29,36] The additional strain-induced contribution to H_a of the multilayer system can then be described in an effective manner by the expression

$$H_{a,\sigma} = (3\,\lambda_s \sigma)/(\mu_0 M_s), \tag{1}$$

where σ is the uniaxial stress experienced by the magnetic material, and M_s is the saturation magnetization. The maximum strain applied, estimated by considering purely geometrical factors, was 0.4%, which lies within the range that was estimated in other studies on thicker Si substrates.[26,37] By fitting the experimental data (Fig. 3(b)) to Eq. (1), assuming $M_s = 8.59 \times 10^5$ A/m and a fracture point for Si at $\sigma \approx 325$ MPa,[34] we obtain the value for the saturation magnetostriction constant to be $\lambda_s = 1.7 \times 10^{-6}$, which is an effective value for the GMR multilayer structure. This value is within the range of the figures previously reported for individual Ni-Fe thin films.[28,37] This strain induced effect is also reported for GMR multilayers prepared on flexible polymeric supports,[38] but are not observed when the GMR stacks are deposited onto pre-stretched elastomeric rubber membranes.[13,39] The latter is attributed to the formation of wrinkles, which accommodate tensile deformations of the substrate without straining the magnetic layers.

The increased width of the GMR curve is accompanied with a decrease of the slope of its linear part (Fig. 3(c)), which represents the field sensitivity of the magnetoresistive elements. For the samples on 50 and 100 μm thick Si membranes, the slope at the inflexion point of the curves decreases linearly with curvature. This change of the slope of the linear part of the GMR curve with bending should be taken into account when applying such flexible GMR sensorics for magnetic field sensing. In this case, the conditioning electronics should be designed in a way to compensate for this effect.

The robustness of the sensor elements against uninterrupted mechanical deformation was tested by reversibly bending the device on 50 μm Si support (Fig. 4). In this so called cyclic bending experiment, the sample is bent 100 times to the radius of 13 mm. The GMR curves are recorded at each bending cycle, when the sample is flat and in the bent state. Measurements are highly reproducible after 100 cycles and there is no measurable variation in the GMR characteristics of the samples.
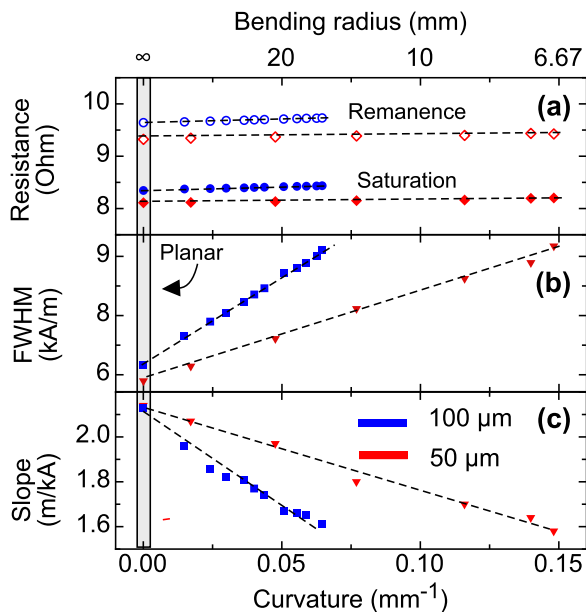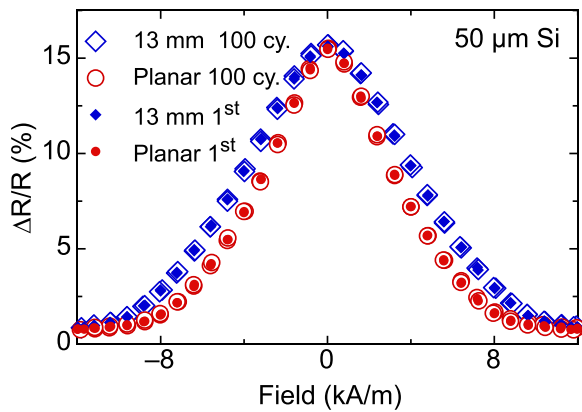

FIG. 3. Impact of bending on the shape of the GMR curves presented in Figs. 2(d) and 2(e). The data of the samples on Si membranes with a thickness of 50 and 100 μm are presented with red and blue symbols, respectively. Lines are guides to the eye. The following parameters are analyzed: (a) resistance measured at remanence and saturation (40 kA/m) corresponding to the maxima and minima of the GMR curve, respectively. (b) FWHM of the GMR curves. (c) Slope of the linear part of the GMR curve taken at the inflexion point.

FIG. 4. Cyclic bending tests carried out of the sample on a $50\,\mu m$ thick Si membrane. GMR curves of the samples in the unbent state (planar) before and after 100 bending cycles are shown with red circles. The data taken of the sample bent to 13 mm radius after the 1st and 100th bending cycle are shown with blue rhombs.

In summary, we fabricated flexible high-performance GMR sensors on Si wafers which are subsequently thinned down to 100 and $50\,\mu m$. The thinning procedure did not alter the properties of the GMR multilayer stacks. We determine that the mechanical bending capabilities of the samples are defined by the thickness of the Si support. The samples prepared on $100\,\mu m$ and $50\,\mu m$ Si membranes can be bent to radii of 15.5 mm and 6.8 mm, respectively. The GMR magnitude is not affected by the bending and remains at $(15.3 \pm 0.4)\%$ for all bending radii and Si membrane thicknesses. This strain invariance of the GMR magnitude is relevant when designing on-off sensors, e.g., magnetic switches, for flexible electronics. As the curvature increased, a broadening of the GMR curve is observed, which is attributed to a strain-induced uniaxial anisotropy imposed by the bending of the Si support. An effective saturation magnetostriction constant for the multilayer stacks of $\lambda_s = 1.7 \times 10^{-6}$ is estimated by the FWHM change of the GMR curved upon bending. The change of the slope of the linear part of the GMR curve upon bending implies that the response of the flexible magnetic field sensors prepared on Si membranes should be corrected by the conditioning electronics prospectively integrated directly on the thinned Si membrane.

[1]J. A. Rogers, M. G. Lagally, and R. G. Nuzzo, Nature **477**, 45 (2011).
[2]S. Bauer, S. Bauer-Gogonea, I. Graz, M. Kaltenbrunner, C. Keplinger, and R. Schwödiauer, Adv. Mater. **26**, 149 (2014).
[3]F. Cavallo and M. G. Lagally, Nanoscale Res. Lett. **7**, 628 (2012).
[4]A. Carlson, A. M. Bowen, Y. Huang, R. G. Nuzzo, and J. A. Rogers, Adv. Mater. **24**, 5284 (2012).
[5]J. A. Rogers, Z. Bao, K. Baldwin, A. Dodabalapur, B. Crone, V. R. Raju, V. Kuck, H. Katz, K. Amundson, J. Ewing, and P. Drzaic, Proc. Natl. Acad. Sci. U.S.A. **98**, 4835–4840 (2001).
[6]M. Kaltenbrunner, T. Sekitani, J. Reeder, T. Yokota, K. Kuribara, T. Tokuhara, M. Drack, R. Schwödiauer, I. Graz, S. Bauer-Gogonea, S. Bauer, and T. Someya, Nature **499**, 458 (2013).
[7]D. H. Kim, N. Lu, R. Ma, Y. S. Kim, R. H. Kim, S. Wang, J. Wu, S. M. Won, H. Tao, A. Islam, K. J. Yu, T. I. Kim, R. Chowdhury, M. Ying, L. Xu, M. Li, H. J. Chung, H. Keum, M. McCormick, P. Liu, Y. W. Zhang, F. G. Omenetto, Y. Huang, T. Coleman, and J. A. Rogers, Science **333**, 838 (2011).
[8]D. H. Kim, J. Viventi, J. J. Amsden, J. Xiao, L. Vigeland, Y. S. Kim, J. A. Blanco, B. Panilaitis, E. S. Frechette, D. Contreras, D. L. Kaplan, F. G. Omenetto, Y. Huang, K. C. Hwang, M. R. Zakin, B. Litt, and J. A. Rogers, Nat. Mater. **9**, 511 (2010).
[9]D. H. Kim, R. Ghaffari, N. Lu, S. Wang, S. P. Lee, H. Keum, R. D'Angelo, L. Klinker, Y. Su, C. Lu, Y. S. Kim, A. Ameen, Y. Li, Y. Zhang, B. de Graff, Y. Y. Hsu, Z. Liu, J. Ruskin, L. Xu, C. Lu, F. G. Omenetto, Y. Huang, M. Mansour, M. J. Slepian, and J. A. Rogers, Proc. Natl. Acad. Sci. U.S.A. **109**, 19910 (2012).
[10]F.-R. Fan, L. Lin, G. Zhu, W. Wu, R. Zhang, and Z. L. Wang, Nano Lett. **12**, 3109 (2012).
[11]M. Melzer, J. I. Mönch, D. Makarov, Y. Zabila, G. S. Canon Bermudez, D. Karnaushenko, S. Baunack, F. Bahr, C. Yan, M. Kaltenbrunner, and O. G. Schmidt, Adv. Mater. **27**, 1274 (2015).
[12]S. S. P. Parkin, K. P. Roche, and T. Suzuki, Jpn. J. Appl. Phys., Part 2 **31**, L1246 (1992).
[13]M. Melzer, D. Makarov, A. Calvimontes, D. Karnaushenko, S. Baunak, R. Kaltofen, Y. Mei, and O. G. Schmidt, Nano Lett. **11**, 2522 (2011).
[14]M. Melzer, D. Karnaushenko, G. Lin, S. Baunack, D. Makarov, and O. G. Schmidt, Adv. Mater. **27**, 1333 (2015).
[15]S. S. P. Parkin, Appl. Phys. Lett. **69**, 3092 (1996).
[16]M. Melzer, G. Lin, D. Makarov, and O. G. Schmidt, Adv. Mater. **24**, 6468 (2012).
[17]C. Barraud, C. Deranlot, P. Seneor, R. Mattana, B. Dlubak, S. Fusil, K. Bouzehouane, D. Deneuve, F. Petroff, and A. Fert, Appl. Phys. Lett. **96**, 072502 (2010).
[18]A. Bedoya-Pinto, M. Donolato, M. Gobbi, L. E. Hueso, and P. Vavassori, Appl. Phys. Lett. **104**, 062412 (2014).
[19]G. Lin, D. Makarov, M. Melzer, W. Si, C. Yan, and O. G. Schmidt, Lab Chip **14**, 4050 (2014).
[20]M. Melzer, M. Kaltenbrunner, D. Makarov, D. Karnaushenko, D. Karnaushenko, T. Sekitani, T. Someya, and O. G. Schmidt, Nat. Commun. **6**, 6080 (2015).
[21]D. Karnaushenko, D. Makarov, C. Yan, R. Streubel, and O. G. Schmidt, Adv. Mater. **24**, 4518 (2012).
[22]D. Karnaushenko, D. Makarov, M. Stöber, D. D. Karnaushenko, S. Baunack, and O. G. Schmidt, Adv. Mater. **27**, 880 (2015).
[23]N. Wacker, H. Richter, M.-U. Hassan, H. Rempp, and J. N. Burghartz, Solid State Electron. **57**, 52 (2011).
[24]D. Shahrjerdi and S. W. Bedell, Nano Lett. **13**, 315 (2013).
[25]M. Löhndorf, T. A. Duenas, A. Ludwig, M. Ruhrig, J. Wecker, D. Burgler, P. Grunberg, and E. Quandt, IEEE Trans. Magn. **38**, 2826 (2002).
[26]M. Löhndorf, T. Duenas, M. Tewes, E. Quandt, M. Ruhrig, and J. Wecker, Appl. Phys. Lett. **81**, 313 (2002).
[27]L. Baril, B. Gurney, D. Wilhoit, and V. Speriosu, J. Appl. Phys. **85**, 5139 (1999).
[28]C.-Y. Hung, M. Mao, S. Funada, T. Schneider, L. Miloslavsky, M. Miller, C. Qian, and H. C. Tong, J. Appl. Phys. **87**, 6618 (2000).
[29]M. P. Hollingworth, M. R. J. Gibbs, and S. J. Murdoch, J. Appl. Phys. **94**, 7235 (2003).
[30]C. Zysset, N. Munzenrieder, L. Petti, L. Buthe, G. A. Salvatore, and G. Troster, IEEE Electron Device Lett. **34**, 1394 (2013).
[31]G. A. Salvatore, N. Münzenrieder, T. Kinkeldei, L. Petti, C. Zysset, I. Strebel, L. Büthe, and G. Tröster, Nat. Commun. **5**, 2982 (2014).
[32]S.-I. Park, J.-H. Ahn, X. Feng, S. Wang, Y. Huang, and J. A. Rogers, Adv. Funct. Mater. **18**, 2673 (2008).
[33]K. P. Wang, Y. Huang, A. Chandra, and K. X. Hu, IEEE Trans. Compon. Packag. Technol. **23**, 309 (2000).
[34]N. Wacker, H. Richter, T. Hoang, P. Gazdzicki, M. Schulze, E. A. Angelopoulos, M-U. Hassan, and J. N. Burghartz, Semicond. Sci. Technol. **29**, 095007 (2014).

[35]R. Coehoorn, "Giant magnetoresistance and magnetic interactions in exchange-biased spin valves," in *Handbook of Magnetic Materials*, edited by K. H. J. Buschow (Elsevier, Amsterdam 2003), Vol. 15.

[36]C. S. Gudeman, IEEE Trans. Magn. **26**, 2580 (1990).

[37]T. J. Gafron, S. E. Russek, and S. L. Burkett, J. Vac. Sci. Technol. A **19**, 1195 (2001).

[38]Y.-F. Chen, Y. Mei, R. Kaltofen, J. I. Mönch, J. Schumann, J. Freudenberger, H.-J. Klauss, and O. G. Schmidt, Adv. Mater. **20**, 3224 (2008).

[39]M. Melzer, D. Karnaushenko, D. Makarov, L. Baraban, A. Calvimontes, I. Mönch, R. Kaltofen, Y. Mei, and O. G. Schmidt, RSC Adv. **2**, 2284 (2012).